

# Terahertz spectroscopy of electromagnons in $\text{Eu}_{1-x}\text{Y}_x\text{MnO}_3$

A. Pimenov,<sup>1</sup> A. Loidl,<sup>2</sup> A. A. Mukhin,<sup>3</sup> V.D. Travkin,<sup>3</sup> V.Yu. Ivanov,<sup>3</sup> and A. M. Balbashov<sup>4</sup>

<sup>1</sup>*Experimentelle Physik IV, Universität Würzburg, 97074 Würzburg, Germany*

<sup>2</sup>*Experimentalphysik V, EKM, University of Augsburg, 86135 Augsburg, Germany*

<sup>3</sup>*General Physics Institute of the Russian Acad. of Sciences, 119991 Moscow, Russia*

<sup>4</sup>*Moscow Power Engineering Institute, 105835 Moscow, Russia*

(Dated: November 30, 2018)

Dielectric permittivity spectra of yttrium-doped  $\text{EuMnO}_3$  in the composition range  $0 \leq x \leq 0.5$  have been investigated in the terahertz frequency range. Magnetoelectric contributions to the permittivity were observed in all compositions for ac electric fields parallel to the crystallographic a-axis. Well defined electromagnons exist for  $x \geq 0.2$  close to  $\nu \sim 20 \text{ cm}^{-1}$  and with dielectric strength strongly increasing on doping. In addition to electromagnons, a broad contribution of magnetoelectric origin is observed for all compositions. For  $\text{Eu}_{0.8}\text{Y}_{0.2}\text{MnO}_3$  the electromagnons can be suppressed by external magnetic fields which induce a canted antiferromagnetic phase. Magnetoelectric effects in the different doping regimes are discussed in detail.

## I. INTRODUCTION

Electric and magnetic properties in most cases are well separated in the physics of the solid state. However, as can be expected already from the Maxwell equations, the cross-coupling effects between electricity and magnetism may exist under appropriate symmetry conditions. This cross-coupling has been pointed out already by Pierre Curie [1] and was later called magnetoelectric (ME) effect. ME effects can be observed e.g. as changes in the electric polarization in external magnetic fields or as electric-field dependence of the magnetic moment. Among the systems revealing the ME effect special interest is drawn to materials with the simultaneous occurrence of (anti-)ferromagnetism and ferroelectricity, which are termed multiferroics [2]. In addition to unusual physical properties the multiferroics are also attractive from the point of view of possible applications [3, 4, 5], e.g. as novel memory elements and optical switches. Multiferroic behavior occurs in a variety of systems originating from very different physical mechanisms, including materials with independent magnetic and ferroelectric subsystems, like some boracites, Aurivillius phases, hexagonal manganites, and the lone-pair ferroelectrics with magnetic ions [5]. Finally, in some perovskite manganites like  $\text{TbMnO}_3$  or  $\text{GdMnO}_3$  it was proven experimentally [6, 7] that the onset of helical magnetic order induces spontaneous ferroelectric (FE) polarization [8, 9]. Dzyaloshinskii-Moriya type interactions have been utilized to explain the ferroelectricity which is induced by the helical spin structure [10, 11, 12]. A similar spin-driven ferroelectricity is believed to be operative in  $\text{Ni}_3\text{V}_2\text{O}_8$  [13].

The existence of an additional energy scale in ME compounds can lead to the appearance of corresponding excitation of ME origin. Recently, such excitations, called electromagnons, have been observed experimentally [14, 15] and it has been shown that electromagnons are the relevant collective ME modes in these materials. Electromagnons are strongly renormalized spin waves

which are coupled to optical phonons and can be excited by an ac electric field. In  $\text{TbMnO}_3$  and  $\text{GdMnO}_3$  it has been documented that these new excitations exist not only in the magnetic phase characterized by the helical spin structure, but also in the longitudinally modulated (sinusoidal) structure, provided that a "helical-type" vector component of the spin-wave is dynamically induced via the ac electric field [14, 16]. The appearance of electromagnons is supported by a theoretical modelling of elementary excitations in helical magnets [17] and by a polaron-like excitation scheme of coupled phonons and magnons [18]. In addition to re-normalized phonons a new excitation has been predicted for the ME state which originates from magnons and reveals a frequency proportional to  $\sqrt{SJD}$ , where  $S$  is the spin value,  $J$  the exchange coupling and  $D$  the magnetic anisotropy. The coupling between electromagnons and phonons has been verified experimentally for  $\text{GdMnO}_3$  [16] and for  $\text{Eu}_{0.75}\text{Y}_{0.25}\text{MnO}_3$  [19].

The analysis of the novel excitations in perovskite multiferroics like  $\text{TbMnO}_3$  still remains complicated due to the interplay between the magnetic sublattices of the manganese and of the rare earth ions. Further difficulties arise e.g. in  $\text{GdMnO}_3$  as this compound is close to a metastable ground state [16, 20] and can hardly be investigated using neutron scattering due to strong absorption. Therefore, the details of the magnetic structure especially in the ME-relevant incommensurate phases remains unknown. To solve these problems, it is of interest to investigate materials without the additional complexity of the rare earth magnetism. The system  $\text{Eu}_{1-x}\text{Y}_x\text{MnO}_3$  is a relevant magnetoelectric compound without rare earth magnetism since  $\text{Mn}^{3+}$  is the only magnetic ion. In addition, yttrium doping allows a continuous tuning of the magnetoelectric properties in this system and seems to increase the strength of the ME coupling [21, 22].

In this paper we present detailed investigations of the terahertz spectra of yttrium-doped  $\text{Eu}_{1-x}\text{Y}_x\text{MnO}_3$  in the concentration range  $0 \leq x \leq 0.5$ . Because the characteristic energies of the magnetoelectric contribution in per-

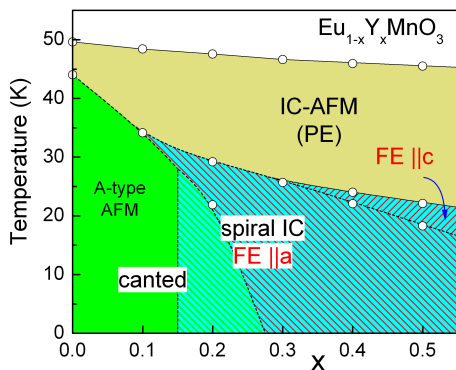


FIG. 1: (T-x) phase diagram of  $\text{Eu}_{1-x}\text{Y}_x\text{MnO}_3$  reproduced from Ref. [21]. The notation of different magnetic phases is given on the basis of magnetization data. AFM - antiferromagnetic phase, IC - incommensurate, PE - paraelectric, FE - ferroelectric. Exact magnetic structures of different phases is still unknown and is indicated in analogy to other perovskite multiferroics.

ovskite manganites lie in the terahertz frequency range, this region is especially important to prove the existence of electromagnons and to study the spectral changes of the ME contribution with doping.

## II. EXPERIMENTAL DETAILS

Single crystals of  $\text{Eu}_{1-x}\text{Y}_x\text{MnO}_3$  have been grown using the floating-zone method with radiation heating. The samples were characterized using X-ray, magnetic and dielectric measurements [21]. The transmittance experiments at terahertz frequencies ( $3 \text{ cm}^{-1} < \nu < 40 \text{ cm}^{-1}$ ) were carried out in a Mach-Zehnder interferometer arrangement [23] which allows measurements of amplitude and phase shift in a geometry with controlled polarization of the radiation. The absolute values of the complex dielectric permittivity  $\varepsilon^* = \varepsilon_1 + i\varepsilon_2$  were determined directly from the measured spectra using the Fresnel optical formulas for the complex transmission coefficient. The experiments in external magnetic fields were performed in a superconducting split-coil magnet with polypropylene windows allowing to carry out transmittance and phase shift experiments in magnetic fields up to 7 T.

## III. RESULTS

Figure 1 reproduces the phase diagram of Y-doped  $\text{EuMnO}_3$  from Ref. [21] which has been obtained using structural, magnetic, dielectric and thermodynamic experiments. In the doping range  $0 \leq x \leq 0.5$   $\text{Eu}_{1-x}\text{Y}_x\text{MnO}_3$  orders antiferromagnetically between 45 and 50 K only slightly depending upon the yttrium content. From the point of view of the magnetodielectric effect (i.e. changes in dielectric permittivity by

magnetic field) and the observation of electromagnons, the phase diagram presented can be divided into four regimes, which we will characterize separately. i) In the low-doping range  $0 \leq x \leq 0.1$  in the incommensurate (IC) antiferromagnetic (AFM) phase weak ME effects are observed and the electromagnons are over-damped and not well defined. The IC-AFM phase in this region is followed by the canted (CA) antiferromagnetic phase which shows no magnetoelectric effect. ii) For Y-doping around  $x = 0.2$  the electromagnons are clearly observed in the spectra and can be suppressed by external magnetic fields, which leads to strong magnetic field-dependence of the dielectric permittivity. iii) For  $x \approx 0.3$  the electromagnons are strong in the ferroelectric (FE) phase at low temperatures but they are not sensitive to external magnetic fields up to 7 T. iv) The region  $0.4 \leq x \leq 0.5$  is closely similar to  $x \approx 0.3$ , but here the dielectric permittivity is weakly dependent upon the external magnetic field in the narrow temperature range of the competition between ferroelectric phases with electric polarization parallel to a- and c-axes, respectively.

Within the accuracy of the present experiments nonzero ME contribution has been observed for  $\vec{e}||a$ -axis only and no effects could be detected for other crystallographic directions. Therefore, only the a-axis results will be presented below.

### A. Weakly-magnetoelectric region ( $x \leq 0.1$ )

The properties of  $\text{Eu}_{0.9}\text{Y}_{0.1}\text{MnO}_3$  are representative for this doping range and similar results have been obtained for pure  $\text{EuMnO}_3$  as well. Figure 2 shows the temperature dependence of the dielectric permittivity of  $\text{Eu}_{0.9}\text{Y}_{0.1}\text{MnO}_3$  in zero magnetic field and in static field of  $\mu_0 H = 4 \text{ T}$  parallel to the c-axis. The steps in the dielectric constant both in real and imaginary parts are observed close to  $T_{IC-CA} \simeq 34 \text{ K}$ . Higher dielectric constant and stronger absorption in the high-temperature incommensurate magnetic phase reflects the existence of additional contributions from the magnetoelectric interactions. These additional contributions are absent in the canted antiferromagnetic (CA-AFM) phase, which explains lower dielectric constant below  $T_{IC-CA} \simeq 34 \text{ K}$ . The shift of the IC-CA phase transition by the static field is well seen in this representation. Because the canted antiferromagnetic phase contains a weak ferromagnetic component parallel to the c-axis, the application of a strong external magnetic field in this direction favors the CA-AFM phase and shifts the phase transition to higher temperatures. No such effects have been observed for other direction of the static magnetic field.

In analogy to the spectral properties of the magnetoelectric phases in  $\text{GdMnO}_3$  and  $\text{TbMnO}_3$  where weak but distinct electromagnons exist already in the IC phase [14], we could expect the existence of characteristic excitations (electromagnons), which govern the magnetoelectric properties in ME materials. In order to prove this

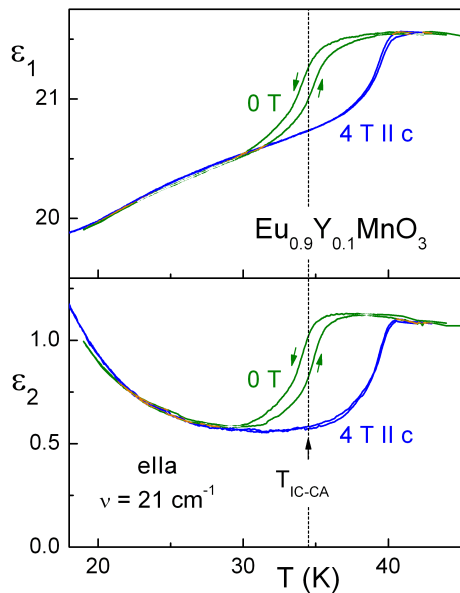


FIG. 2: Temperature dependence of the a-axis dielectric permittivity of  $\text{Eu}_{0.9}\text{Y}_{0.1}\text{MnO}_3$  in zero external field (green) and at  $\mu_0 H = 4 \text{ T}$  along the c-axis (blue). Upper panel - real part, lower panel - imaginary part.  $T_{\text{IC-CA}}$  indicates the transition between the incommensurate and canted antiferromagnetic states. This temperature has been obtained from the magnetization experiments

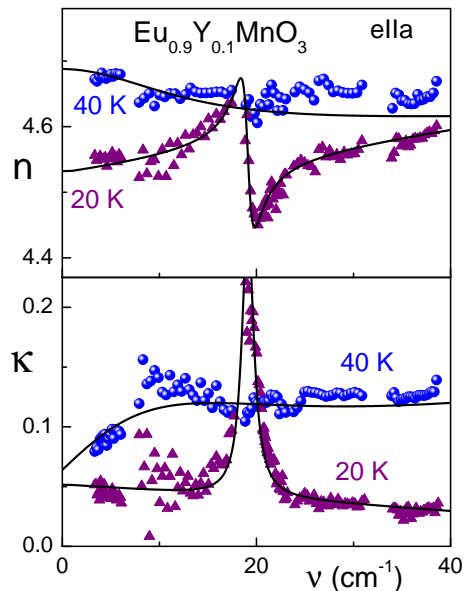


FIG. 3: Terahertz spectra of  $\text{Eu}_{0.9}\text{Y}_{0.1}\text{MnO}_3$  in incommensurate (40 K data) and canted (20 K data) antiferromagnetic phases. Upper panel - refractive index, lower panel - absorption coefficient. Narrow mode at  $\nu \simeq 19 \text{ cm}^{-1}$  represent the antiferromagnetic resonance. Broad additional absorption for  $T = 40 \text{ K}$  is of magnetoelectric origin. Symbols represent experimental data, lines show the fits using the sum of Lorentzians and a Debye relaxator.

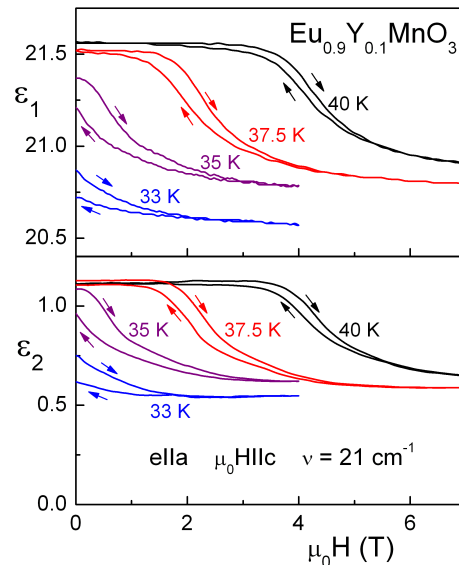


FIG. 4: Magnetic field dependence of dielectric permittivity of  $\text{Eu}_{0.9}\text{Y}_{0.1}\text{MnO}_3$  close to the IC-CA transition between two antiferromagnetic phases. Upper panel shows the real part, lower panel - imaginary part.

similarly the terahertz spectra of  $\text{Eu}_{0.9}\text{Y}_{0.1}\text{MnO}_3$  have been measured in the IC and CA-AFM phases. Typical results of these experiments are shown in Fig. 3. A strong and narrow absorption mode is observed in these spectra close to  $19 \text{ cm}^{-1}$  in the CA-AFM phase (20 K data). This excitation represents the antiferromagnetic resonance (AFMR), which for the studied polarization of ac magnetic field ( $\vec{h}||c$ , b-cut sample) corresponds to the quasiantiferromagnetic mode of the canted antiferromagnetic phases [24] and is well documented e.g. in  $\text{La}_{1-x}\text{Sr}_x\text{MnO}_3$  [25]. The AFMR mode is of magnetic origin and therefore cannot be plotted together with the spectra of dielectric permittivity. Therefore, the  $(n, \kappa)$  representation has been chosen in this case, where  $n + i\kappa = \sqrt{\varepsilon^* \mu^*}$ . However, far from the AFMR mode the response is purely dielectric and the dielectric permittivity can be calculated as  $\text{Re}(\varepsilon) \simeq n^2$  and  $\text{Im}(\varepsilon) \simeq 2n\kappa$ . In this approximation the upper panel of Fig. 3 reflects qualitatively the behavior of  $\varepsilon_1$  and the lower panel of  $\varepsilon_2$ , respectively. Comparing the spectra at 20 K and at 40 K clear additional contribution can be seen in the magneto-electric IC-phase. This is seen both as a broad absorption in the spectra of  $\kappa(\nu)$ , and as increased low-frequency values of the refractive index in the IC-phase. Comparing this spectra to that of  $\text{GdMnO}_3$  and  $\text{TbMnO}_3$  [14], this additional contribution closely resembles electromagnon-like excitations. However, in the case of  $\text{Eu}_{0.9}\text{Y}_{0.1}\text{MnO}_3$  electromagnons are not well-defined in energy and are seen as broad contribution only. By fitting the spectra using a Debye-like relaxator (solid lines in Fig. 3,  $T = 40 \text{ K}$ ), the characteristic frequency of the ME-excitation in  $\text{Eu}_{0.9}\text{Y}_{0.1}\text{MnO}_3$  can be estimated as  $\nu \sim 10 \text{ cm}^{-1}$ . Of course in this case this characteristic frequency corre-

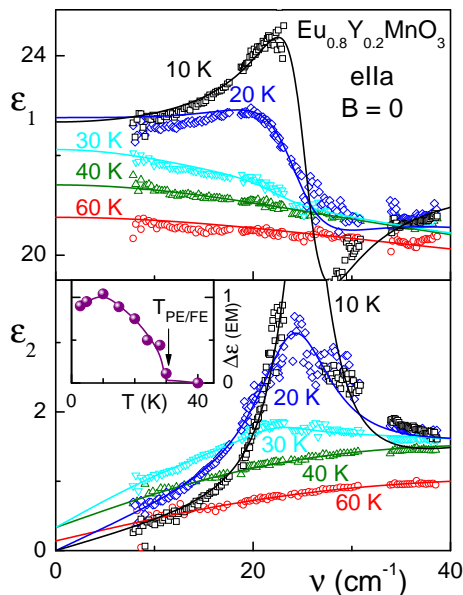


FIG. 5: Spectra of the dielectric permittivity along the  $a$ -axis of  $\text{Eu}_{0.8}\text{Y}_{0.2}\text{MnO}_3$  in the terahertz frequency range and without external magnetic field. Upper panel - real part, lower panel - imaginary part. Symbols - experiment, lines - Lorentzian fit. Inset shows the dielectric contribution of electromagnon at  $\nu \simeq 24 \text{ cm}^{-1}$ .

sponds to an inverse mean lifetime of the excitations.

In the vicinity of the IC-CA transition in  $\text{Eu}_{0.9}\text{Y}_{0.1}\text{MnO}_3$  the magnetoelectric contribution is unstable against external magnetic fields along the  $c$ -axis, because the application of the magnetic field in this direction favors the CA-AFM phase. In this temperature range the ME effects can be observed at terahertz frequencies. The results of ME experiments are represented in Fig. 4 which shows real and imaginary parts of the dielectric constant as function of external magnetic field. In the temperature range  $35 \text{ K} \lesssim T \lesssim 40 \text{ K}$  the dielectric properties can be easily switched between the values corresponding to IC and CA-phases. The observed changes in the permittivity correspond well to the difference between the spectra of both phases as shown in Fig. 3.

### B. Intermediate doping range ( $x \sim 0.2$ )

For  $\text{Eu}_{1-x}\text{Y}_x\text{MnO}_3$  being close to  $x = 0.2$  the collinear spin order for  $T < T_N$  is not ferroelectric, but for  $T \leq 29 \text{ K}$  it is followed by a spiral spin structure which induces ferroelectricity with the polarization  $P \parallel a$  [21]. It is important to note that this spiral spin structure reveals a ferromagnetic component, probably due to a conical-like distortion [21]. Although the amplitude of the magnetoelectric effects in this compound  $\Delta\epsilon_1(H)$  is only slightly stronger than in  $\text{Eu}_{0.9}\text{Y}_{0.1}\text{MnO}_3$ , electromagnons can be clearly observed in the spectra and can be well fitted

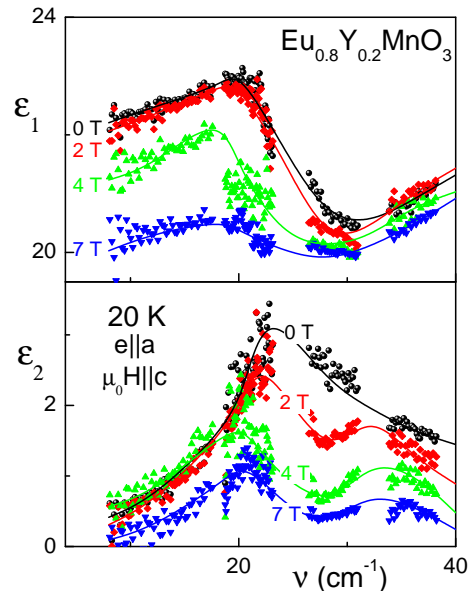


FIG. 6: Suppression and splitting of electromagnon in external magnetic field in the  $a$ -axis dielectric spectra of  $\text{Eu}_{0.8}\text{Y}_{0.2}\text{MnO}_3$ . Upper panel - real part, lower panel - imaginary part. Symbols - experiment, lines - Lorentzian fit.

with a Lorentzian with an eigenfrequency close to  $\nu \simeq 24 \text{ cm}^{-1}$  (Fig. 5). Figure 5 shows real and imaginary parts of the dielectric spectra of  $\text{Eu}_{0.8}\text{Y}_{0.2}\text{MnO}_3$  at different temperatures and in zero external magnetic field. Already with the onset of the IC collinear phase at  $T \simeq 48 \text{ K}$  a broad terahertz absorption starts to grow and marks an approaching of the FE state. The dielectric spectra can be fitted using a Debye relaxator with characteristic frequency of roughly  $25 \text{ cm}^{-1}$ . In addition to this broad contribution, a well-defined electromagnon appears in the FE state below  $T = 29 \text{ K}$ , which corresponds to the phase transition from the paraelectric (PE) into the ferroelectric (FE) state. The inset in the lower panel of Fig. 5 shows the dielectric contribution of the electromagnon which exists in the ferroelectric phase only. The growth of the spectral weight of the electromagnon takes place on the costs of the relaxator that nevertheless survives up to the lowest temperatures.

$\text{Eu}_{0.8}\text{Y}_{0.2}\text{MnO}_3$  reveals close similarities with the magnetoelectric properties of  $\text{GdMnO}_3$  and  $\text{TbMnO}_3$ . This comprises characteristic frequency of electromagnon, typical values of the dielectric permittivity, and includes the possibility to suppress the electromagnon using external magnetic fields. Figure 6 shows the dielectric spectra of  $\text{Eu}_{0.8}\text{Y}_{0.2}\text{MnO}_3$  for different external magnetic fields parallel to the  $c$ -axis. Compared to  $\text{GdMnO}_3$  and  $\text{TbMnO}_3$  the suppression of the magnetoelectric contribution is more gradual and is not fully finished even at  $\mu_0 H = 7 \text{ T}$ . This difference could be due to the fact that the FE phase of  $\text{Eu}_{0.8}\text{Y}_{0.2}\text{MnO}_3$  exhibits a ferromagnetic component and a different field dependence compared to the pure antiferromagnetic spiral can be expected. In addi-

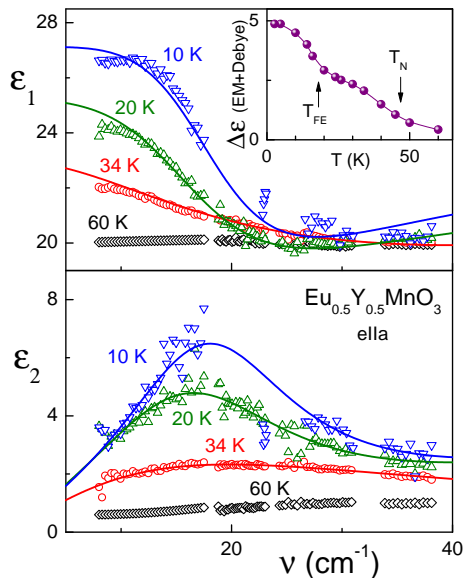


FIG. 7: Spectra of dielectric permittivity along the a-axis of  $\text{Eu}_{0.5}\text{Y}_{0.5}\text{MnO}_3$  in the terahertz frequency range. Upper panel - real part, lower panel - imaginary part. Symbols - experiment, lines - Lorentzian fit. Inset shows the dielectric contribution of electromagnon and of Debye relaxator.

tion, fine structure of the residual absorption is observed in the spectra and can be approximated by two excitations at  $21\text{ cm}^{-1}$  and  $34\text{ cm}^{-1}$ , respectively.

It seems that the spectra of the magnetoelectric perovskite manganites cannot be described using just one single electromagnon and further components can be separated in the spectra. In addition to the splitting of electromagnon observed in Fig. 6, the above-mentioned Debye-like contribution can be seen in all spectra of  $\text{Eu}_{1-x}\text{Y}_x\text{MnO}_3$ . This contribution was dominating for  $\text{Eu}_{0.9}\text{Y}_{0.1}\text{MnO}_3$  and in  $\text{Eu}_{0.8}\text{Y}_{0.2}\text{MnO}_3$  it gradually transfers its spectral weight into electromagnons. Complicated spectra of electromagnons have been observed in  $\text{TbMnO}_3$  as well, both in dielectric permittivity [14] and in inelastic neutron scattering experiments [26]. Finally, recent FIR experiments in  $\text{Eu}_{0.75}\text{Y}_{0.25}\text{MnO}_3$  [19] revealed the existence of further electromagnon around  $\nu_2 = 80\text{ cm}^{-1}$  in addition to a low-frequency electromagnon at  $\nu_1 = 25\text{ cm}^{-1}$ .

### C. Ferroelectric range ( $x \geq 0.3$ )

In this doping region and in zero external magnetic field the permittivity spectra similar to  $\text{Eu}_{0.8}\text{Y}_{0.2}\text{MnO}_3$  have been observed. A typical example of these spectra is represented in Fig. 7 which shows real and imaginary parts of the dielectric permittivity of  $\text{Eu}_{0.5}\text{Y}_{0.5}\text{MnO}_3$  for  $\vec{\epsilon}||a$ . Similar to other compositions, broad Debye-like contribution of ME origin can be observed on entering the IC phase. This excitation is getting more pronounced below  $T_N \simeq 46\text{ K}$  and its characteristic damping frequency

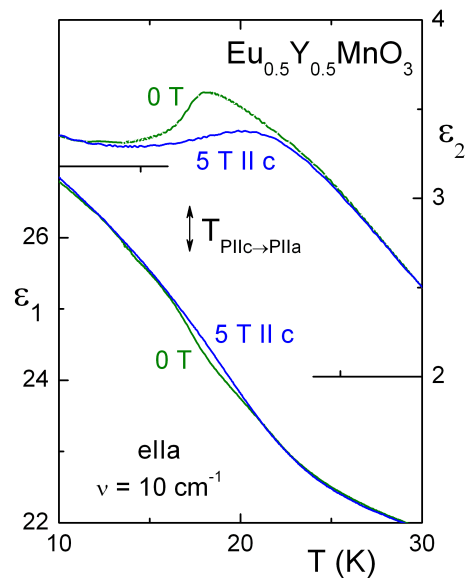


FIG. 8: Temperature dependence of the a-axis dielectric permittivity of  $\text{Eu}_{0.5}\text{Y}_{0.5}\text{MnO}_3$  in zero external field and at  $\mu_0 H = 5\text{ T}$  along the c-axis. Upper panel - real part, lower panel - imaginary part. Narrow region close to  $T = 18\text{ K}$ , where the permittivity is sensitive to magnetic field, corresponds to the ferroelectric phase with  $P||c$ .

can be roughly identified as  $\Gamma \sim 20\text{ cm}^{-1}$ . Temperature dependence of this additional magnetoelectric contribution is shown in the inset to the upper frame of Fig. 7. Especially below the transition from the paraelectric to the ferroelectric phase at  $T_{PE/FE} \sim 20\text{ K}$  this contribution transforms to a well-defined electromagnon with a characteristic maximum in  $\epsilon_2$  and a step in  $\epsilon_1$  close to  $17\text{ cm}^{-1}$  corresponding to its eigenfrequency. The transition to the ferroelectric phase is also seen as a change in slope in the temperature dependence of the dielectric contribution of the electromagnon (inset to Fig. 7). We note that the dielectric contribution of the electromagnons in this composition range is the strongest for the Y-doping range investigated.

For the composition  $\text{Eu}_{0.7}\text{Y}_{0.3}\text{MnO}_3$  no magnetic field dependence of the dielectric properties could be observed for external magnetic fields  $\mu_0 H \leq 7\text{ T}$  within the experimental accuracy. However, for  $x \geq 0.4$  a narrow temperature region with  $P||c$  exists (Fig. 1) which can be influenced by magnetic fields  $\mu_0 H||c$ . Although this effect is extremely weak, it can be observed in the temperature dependence of the dielectric permittivity. Figure 8 shows the dielectric permittivity of  $\text{Eu}_{0.5}\text{Y}_{0.5}\text{MnO}_3$  at  $\nu = 10\text{ cm}^{-1}$  as function of temperature in zero external magnetic field and in a field of 5T parallel to the c-axis. A clear hallmark of the phase transition to the ferroelectric phase with  $P||a$  is seen close to 17 K. This transition is accompanied by a change of the rotation plane of the spiral spin structure from the bc-plane (with  $P||c$ ) to the ab-plane (with  $P||a$ ). In an external magnetic field with  $\mu_0 H||c$  stabilizing the spiral structure with  $P||a$ , the on-

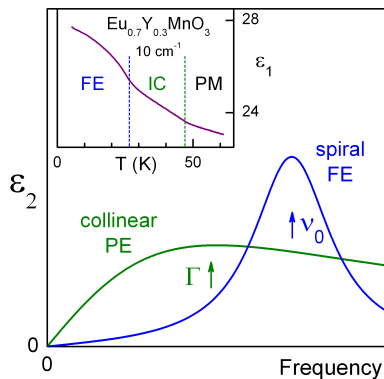


FIG. 9: Schematic representation of the terahertz spectra of magnetolectric manganites. Paramagnetic (PM) phase - no magnetolectric contribution, collinear incommensurate phase (paraelectric (PE)) - broad Debye-like response, spiral ferroelectric (FE) phase - well-defined electromagnons.  $\Gamma$  is the damping of the relaxator,  $\nu_0$  is the eigenfrequency of the electromagnon, and IC indicates the incommensurate antiferromagnetic (collinear) phase. The inset shows the temperature dependence of the low-frequency dielectric constant of  $\text{Eu}_{0.7}\text{Y}_{0.3}\text{MnO}_3$  as an illustration of the discussed behavior. Changes in slope in the temperature dependence correspond well to the phase transitions to the IC and FE states.

set of the transition to this phase is shifted to higher temperatures up to  $T_{PE/FE}$ . This results in a suppression the  $P||c$  phase and in weak magnetodielectric effects ( $\Delta\epsilon_1(H)/\epsilon_1(0) \sim 0.8\%$  in the real part of the dielectric permittivity, Fig. 8). We note however that compared to the strong effects for low-doping compositions the electromagnon contribution is rigid and remains basically stable against the influence of external magnetic fields.

#### IV. DISCUSSION

Comparing the spectra of the dielectric permittivity of all compositions investigated several similarities exist in the doping series  $\text{Eu}_{1-x}\text{Y}_x\text{MnO}_3$ . General behavior of the terahertz spectra is represented schematically in Fig. 9. Broad magnetolectric contribution exists in the terahertz spectra of the dielectric permittivity in the collinear PE phase in all samples, which seems to result from the same mechanisms as the electromagnon resonance. This contribution can be described using Debye-like relaxation and is observed already in the paramagnetic phase possibly due to magnon-like fluctuations.

In addition to the broad contribution a well defined electromagnon starts to grow in the spiral FE state with a doping-dependent resonant frequency which shifts from  $\nu \simeq 25 \text{ cm}^{-1}$  for  $x = 0.2$  to  $\nu \simeq 18 \text{ cm}^{-1}$  for  $x = 0.5$ . The dielectric contribution of the electromagnon strongly depends upon Y-concentration and grows from  $\Delta\epsilon \simeq 1$  for

$x = 0.2$  to  $\Delta\epsilon \simeq 5$  for  $x = 0.5$ . This reflects the increase of the magnetolectric coupling with the yttrium doping. Indeed, for  $x = 0.2$  the stabilities of the ferroelectric and the canted states are similar and both phases can be easily switched by external magnetic fields. For  $x \geq 0.3$  the FE state is stable at low temperature and the electromagnons cannot be influenced by external magnetic fields.

The interplay of different contribution to the dielectric permittivity can be most clearly seen in the temperature dependence of the low-frequency dielectric permittivity. According to the sum rule [27]

$$\epsilon_1(0) = 1 + \frac{2}{\pi} \int_0^\infty \frac{\epsilon_2(\omega)}{\omega} d\omega \quad (1)$$

the low-frequency dielectric permittivity is a measure of all high frequency contributions. The inset in Fig. 9 shows the temperature dependence of  $\epsilon_1$  in  $\text{Eu}_{0.7}\text{Y}_{0.3}\text{MnO}_3$  at  $\nu = 10 \text{ cm}^{-1}$ , i.e. below all excitations observed in the terahertz spectra. On cooling the sample through  $T_N = 48 \text{ K}$  the increase in the slope of  $\epsilon_1(T)$  reflects the growth of the Debye-like excitation in the collinear PE state. On further cooling, the spiral FE state is reached where well-defined electromagnons are observed. The appearance of this contribution is again observed as a change in slope of  $\epsilon_1(T)$  at  $T_{IC/FE}$ .

Finally, the spectra of electromagnons reveal distinct fine structure. This is most clearly documented in Fig. 6 and correlates well with other experimental observations both in  $\text{TbMnO}_3$  [26] and in  $\text{Eu}_{0.75}\text{Y}_{0.25}\text{MnO}_3$  [19].

#### V. CONCLUSIONS

Dielectric properties of yttrium-doped  $\text{EuMnO}_3$  in the composition range  $0 \leq x \leq 0.5$  have been investigated in the terahertz- frequency range. Nonzero magnetolectric contribution to the dielectric permittivity can be observed in all compositions for  $\vec{e}||a$  only. In the low doping range with coexisting incommensurate and canted antiferromagnetic states ( $x \leq 0.2$ ) the dielectric properties can be modified by external magnetic field parallel to the  $c$ -axis especially on the border line between these two phases. Well defined electromagnons are observed for  $x \geq 0.2$  close to  $\nu \sim 20 \text{ cm}^{-1}$  and with strongly doping-dependent dielectric strength. In addition to electromagnons, a broad contribution of magnetolectric origin is observed for all compositions. Most naturally these contributions can be explained as heavily overdamped electromagnons which already exist in the collinear spin state.

This work has been partly supported by by DFG (SFB 484), and by RFBR (04-02-16592, 06-02-17514).

- 
- [1] P. Curie, *J. Physique* **3**, 393 (1894).
- [2] H. Schmid, *Ferroelectrics* **62**, 317 (1994).
- [3] N. A. Hill, *J. Phys. Chem. B* **104**, 6694 (2000).
- [4] M. Fiebig, *J. Phys. D: Appl. Phys.* **38**, R123 (2005).
- [5] D. Khomskii, *J. Magn. Magn. Mater.* **306**, 1 (2006).
- [6] T. Kimura, T. Goto, H. Shintani, K. Ishizaka, T. Arima, and Y. Tokura, *Nature* **426**, 55 (2003).
- [7] T. Kimura, G. Lawes, T. Goto, Y. Tokura, and A. P. Ramirez, *Phys. Rev. B* **71**, 224425 (2005).
- [8] M. Kenzelmann, A. B. Harris, S. Jonas, C. Broholm, J. Schefer, S. B. Kim, C. L. Zhang, S.-W. Cheong, O. P. Vajk, and J. W. Lynn, *Phys. Rev. Lett.* **95**, 087206 (2005).
- [9] T. Arima, A. Tokunaga, T. Goto, H. Kimura, Y. Noda, and Y. Tokura, *Phys. Rev. Lett.* **96**, 097202 (2006).
- [10] H. Katsura, N. Nagaosa, and A. V. Balatsky, *Phys. Rev. Lett.* **95**, 057205 (2005).
- [11] M. Mostovoy, *Phys. Rev. Lett.* **96**, 067601 (2006).
- [12] I. A. Sergienko and E. Dagotto, *Phys. Rev. B* **73**, 094434 (2006).
- [13] G. Lawes, A. B. Harris, T. Kimura, N. Rogado, R. J. Cava, A. Aharony, O. Entin-Wohlman, T. Yildirim, M. Kenzelmann, C. Broholm, and A. P. Ramirez, *Phys. Rev. Lett.* **95**, 087205 (2005).
- [14] A. Pimenov, A. A. Mukhin, V. Yu. Ivanov, V. D. Travkin, A. M. Balbashov, and A. Loidl, *Nature Physics* **2**, 97 (2006).
- [15] A. B. Sushkov, R. V. Aguilar, S. Park, S.-W. Cheong, and H. D. Drew, *Phys. Rev. Lett.* **98**, 027202 (2007).
- [16] A. Pimenov, T. Rudolf, F. Mayr, A. Loidl, A. A. Mukhin, and A. M. Balbashov, *Phys. Rev. B* **74**, 100403 (2006).
- [17] H. Katsura, A. V. Balatsky, and N. Nagaosa, *Phys. Rev. Lett.* **98**, 027203 (2007).
- [18] I. E. Chupis, cond-mat/0702636 (unpublished).
- [19] R. V. Aguilar, A. B. Sushkov, C. L. Zhang, Y.-J. Choi, S.-W. Cheong, and H. D. Drew, cond-mat/0704.3632 (unpublished).
- [20] J. Hemberger, S. Lobina, H.-A. Krug von Nidda, N. Tristan, V. Yu. Ivanov, A. A. Mukhin, A. M. Balbashov, and A. Loidl, *Phys. Rev. B* **70**, 024414 (2004).
- [21] J. Hemberger, F. Schrettle, A. Pimenov, P. Lunkenheimer, V. Yu. Ivanov, A. A. Mukhin, A. M. Balbashov, and A. Loidl, *Phys. Rev. B* **75**, 035118 (2007).
- [22] V. Yu. Ivanov, A. A. Mukhin, V. D. Travkin, A. S. Prokhorov, A. M. Kadomtsev, Yu. F. Popov, G. P. Vorobei, K. I. Kamilov and A.M. Balbashov, *J. Magn. Magn. Mater.* **300**, e130 (2006).
- [23] A. A. Volkov, Yu. G. Goncharov, G. V. Kozlov, S. P. Lebedev, and A. M. Prochorov, *Infrared Phys.* **25**, 369 (1985); A. Pimenov, S. Tachos, T. Rudolf, A. Loidl, D. Schrupp, M. Sing, R. Claessen, and V. A. M. Brabers, *Phys. Rev. B* **72**, 035131 (2005).
- [24] A. A. Mukhin, A. Pimenov, M. Biberacher, and A. Loidl, *J. Magn. Res.* **170**, 8 (2004).
- [25] D. Ivannikov, M. Biberacher, H.-A. Krug von Nidda, A. Pimenov, A. Loidl, A. A. Mukhin, and A. M. Balbashov, *Phys. Rev. B* **65**, 214422 (2002).
- [26] D. Senff, P. Link, K. Hradil, A. Hiess, L. P. Regnault, Y. Sidis, N. Aliouane, D. N. Argyriou, and M. Braden, *Phys. Rev. Lett.* **98**, 137206 (2007).
- [27] M. Dressel and G. Grüner, *Electrodynamics of Solids: Optical Properties of Electrons in Matter*, (Cambridge University Press, Cambridge, 2002), p.67.